

## Article

# Dual-Exciting Central Carbon Nanoclusters for the Dual-Channel Detection of Hemin

Ya-Ting Gao<sup>1</sup>, Shuai Chang<sup>1</sup>, Bin-Bin Chen<sup>1,2,\*</sup>  and Da-Wei Li<sup>1,\*</sup>

<sup>1</sup> Key Laboratory for Advanced Materials, Shanghai Key Laboratory of Functional Materials Chemistry, Frontiers Science Center for Materiobiology & Dynamic Chemistry, School of Chemistry & Molecular Engineering, East China University of Science and Technology, Shanghai 200237, China; gaoyating@mail.ecust.edu.cn (Y.-T.G.); y12213021@mail.ecust.edu.cn (S.C.)

<sup>2</sup> School of Science and Engineering, Shenzhen Institute of Aggregate Science and Technology, The Chinese University of Hong Kong, Shenzhen, 2001 Longxiang Boulevard, Longgang District, Shenzhen 518172, China

\* Correspondence: chenbinbin\_swu@163.com (B.-B.C.); daweili@ecust.edu.cn (D.-W.L.)

**Abstract:** Constructing optical nanoprobe with superior performance is highly desirable for sensitive and accurate assays. Herein, we develop a facile room-temperature strategy for the fabrication of green emissive carbon nanoclusters (CNCs) with dual-exciting centers for the dual-channel sensing of hemin. The formation of the CNCs is attributed to the crosslinking polymerization of the precursors driven by the Schiff base reaction between ethylenediamine and 2,3-dichloro-5,6-dicyano-1,4-benzoquinone. Most importantly, the proposed CNCs have a unique excitation-independent green emission (518 nm) with two excitation centers at 260 nm (channel 1) and 410 nm (channel 2). The dual-exciting central emission can serve as dual-channel fluorescence (FL) signals for highly sensitive and reliable detection of hemin based on the inner filter effect. Because of the great spectral overlap difference between the absorption spectrum of hemin and the excitation lights of the CNCs in the two channels, hemin has a different quenching effect on FL emission from different channels. The dual-channel signals of the CNCs can detect hemin in the range of 0.075–10  $\mu\text{M}$  (channel 1) and 0.25–10  $\mu\text{M}$  (channel 2), respectively. These findings not only offer new guidance for the facile synthesis of dual-exciting central CNCs but also establish a reliable sensing platform for the analysis of hemin in complex matrixes.



**Citation:** Gao, Y.-T.; Chang, S.; Chen, B.-B.; Li, D.-W. Dual-Exciting Central Carbon Nanoclusters for the Dual-Channel Detection of Hemin.

*Inorganics* **2023**, *11*, 226. <https://doi.org/10.3390/inorganics11060226>

Academic Editor: Zdeněk Slanina

Received: 19 April 2023

Revised: 18 May 2023

Accepted: 21 May 2023

Published: 25 May 2023



**Copyright:** © 2023 by the authors. Licensee MDPI, Basel, Switzerland. This article is an open access article distributed under the terms and conditions of the Creative Commons Attribution (CC BY) license (<https://creativecommons.org/licenses/by/4.0/>).

**Keywords:** carbon nanoclusters; dual-exciting centers; Schiff base reaction; dual-channel detection; hemin

## 1. Introduction

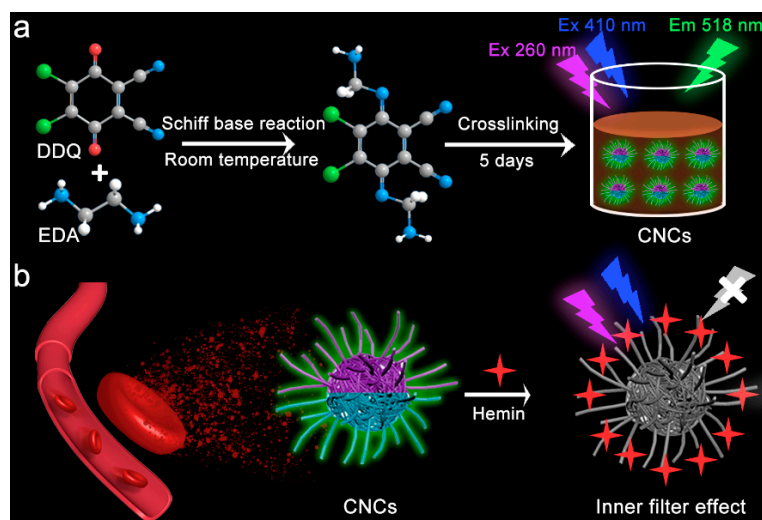
Optical nanoprobe have attracted much attention because of their indispensable role in the field of sensing and imaging [1–3]. In addition to their high sensitivity and selectivity for analytes, excellent nanoprobe usually require a high signal-to-noise ratio to meet the rapidly increasing requirements of food safety, disease diagnosis, environmental analysis, and other fields. Single-signal-based nanoprobe, the most common sensing system, are usually problematic due to the unavoidable interferences during the detection of analytes, such as the non-homogeneous concentration distribution of nanoprobe, light scattering from the sample matrixes, and excitation light fluctuation [4]. In order to overcome these drawbacks, various strategies have been developed to achieve the accurate measurement of analytes, the most common of which is the design of ratiometric fluorescence (FL) and dual-channel sensing probe. Ratiometric FL nanoprobe are attractive for the improvement of signal-to-noise ratio and the accuracy of analysis due to the intrinsic built-in correction [5]. Likewise, dual-channel sensing nanoprobe use dual-channel signals as self-control, which is beneficial for achieving more accurate analysis results [6].

The dual-channel sensing method can combine the advantages of each method and uses the dual-channel signals for self-supervision of detection results, which can improve

the selectivity and accuracy of nanoprobe [7]. Currently, various strategies have been developed for the preparation of nanoprobe with dual-channel response signals. Wang's group [6] developed a colorimetric/electrochemical sensing platform for the detection of aflatoxin B1, with improved analysis precision and reduced false-negative and false-positive rates. Liu's group [8] developed a paper-based sensing system for fluorescent and colorimetric dual-channel determination of foodborne pathogenic bacteria, with more reliable results. Li's group [9] constructed periodic Au@metal-organic framework nanoparticle arrays as dual-channel biosensors for detecting glucose based on the dual signal change of surface plasmon resonance and diffraction peaks. These strategies usually rely on the response signals of a hybrid nanosystem composed of two optical materials that have a complicated and time-consuming preparation process [7]. Moreover, the stability of the hybrid nanosystem is a major obstacle to the development of dual-channel nanoprobe. Therefore, developing a facile strategy for the preparation of dual-channel nanoprobe is very attractive.

Hemin, a well-known natural porphyrinatoiron complex, is an indispensable substance in living organisms, which has important roles in the regulation of oxygen transport, gene expression, hemoglobin synthesis, and other physiological processes [10–12]. Hemin is composed of a porphyrin ring containing four pyrrole molecules and  $\text{Fe}^{3+}$  ions located at the center, which can keep stable in the body as a cofactor of hemoglobin without resulting in hemolysis and inflammation [13]. Hemin is abundant in living organisms mainly as an electron transfer medium according to the reversible redox reaction of  $\text{Fe}^{3+}/\text{Fe}^{2+}$  [14]. Excessive or lack of hemin is not beneficial for human health; this deficiency may cause neuroglobin expression in neural cells and accelerate the formation of endogenous CO, while an excess may lead to permanent brain secondary damage after a hemorrhagic stroke [15]. In addition, hemin can not only serve as a natural iron supplement for the treatment of iron deficiency anemia but also acts as a raw material for the synthesis of semi-synthetic bilirubin and anticancer medicines [16]. Therefore, accurate determination of hemin is of great significance for the early diagnosis of diseases and analysis of medical content. Dual-channel sensing platforms provide a great potential for highly sensitive and reliable detection of hemin, which exhibits incomparable advantages such as more reliable analysis results in comparison to other traditional methods, including chemiluminescence [16], electrochemiluminescence [17], and surface-enhanced Raman scattering [18] techniques.

Luminescent carbon nanoclusters (CNCs) are regarded as a new type of carbon nanomaterial, which has been widely used in numerous fields, such as optical imaging and analysis detection [5]. In contrast to the widely studied single-exciting central CNCs, dual-exciting central CNCs have rarely been reported to date. Our group has developed various quinone-based luminescent nanocarbon materials with different emission properties [19–21], such as dual-emission carbonized polymer dots prepared by using ethylenediamine and tetrachlorobenzoquinone at room temperature [22], whereas CNCs with dual excitation centers have not been reported yet. By changing tetrachlorobenzoquinone to 2,3-dichloro-5,6-dicyano-1,4-benzoquinone (DDQ), for the first time, we developed a facile Schiff base reaction for the preparation of dual-exciting central CNCs by simply keeping the mixture of ethylenediamine (EDA) and DDQ in aqueous solution at room temperature (Scheme 1a). DDQ was chosen as a precursor because its active carbonyl group can react with the amino group of EDA at room temperature to form CNCs through Schiff base polymerization. The proposed CNCs exhibit a unique dual-exciting central emission property: one excitation-independent green emission, but can be excited at two different excitation regions centered at about 260 nm (channel 1) and 410 nm (channel 2), respectively. Because of the difference of spectral overlap, hemin has different FL quenching ability to the two channels of the CNCs (Scheme 1b), achieving a channel-dependent detection range towards hemin, with a linear range of 0.075–10  $\mu\text{M}$  (channel 1) and 0.25–10  $\mu\text{M}$  (channel 2), respectively. This work not only provides a deeper understanding of the optical mechanism of luminescent carbon materials but also develops a reliable dual-channel sensing platform for hemin detection.



**Scheme 1.** Illustration of the room-temperature synthesis of dual-exciting central CNCs using EDA and DDQ and their dual-channel detection of hemin.

## 2. Results and Discussion

### 2.1. Synthesis and Characterization of CNCs

A facile room temperature method is developed for the first time for preparing dual-exciting central CNCs by mixing the EDA and DDQ in an aqueous solution. When EDA and DDQ are mixed together, two active amino groups of the EDA molecule can easily react with the two carbonyl groups of DDQ by Schiff base reaction to form an extended polymer chain [22]. Subsequently, intermolecular interactions enable the polymer chains to be further wound into amorphous CNCs [5]. A high-resolution transmission electron microscope (TEM) image (Figure 1a) exhibits that the proposed CNCs do not have an obvious carbon core or any lattice fringes, indicating their completely amorphous internal structure. The particle statistics result (Figure 1b) shows that the CNCs have a uniform size distribution with an average diameter of  $1.8 \pm 0.2$  nm.

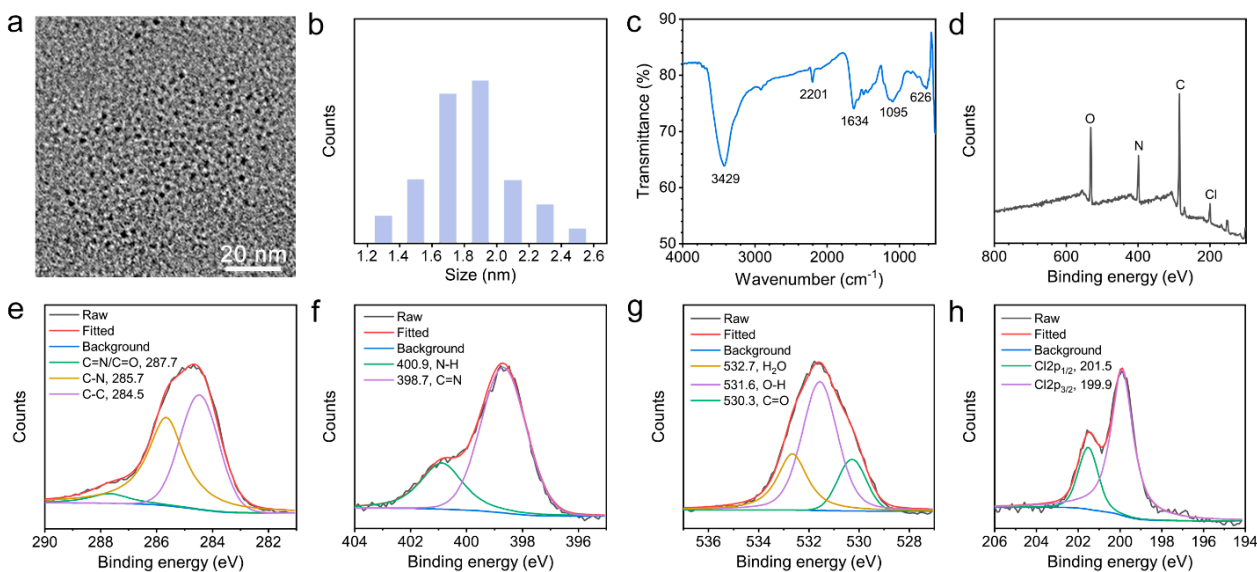


**Figure 1.** Characterization of dual-exciting central CNCs. (a) TEM image, (b) size distribution, (c) FT-IR spectrum, (d) XPS spectrum, (e) C1s spectrum, (f) N1s spectrum, (g) O1s spectrum and (h) Cl2p spectrum of CNCs.

The structural characteristics of the CNCs are further studied by Fourier transform infrared (FT-IR) and X-ray photoelectron spectrometer (XPS) spectra. FT-IR spectrum (Figure 1c) shows that the prepared CNCs have several strong stretching vibration bands of N–H at  $3429\text{ cm}^{-1}$ ,  $\text{C}\equiv\text{N}$  at  $2201\text{ cm}^{-1}$ ,  $\text{C}=\text{N}$  at  $1634\text{ cm}^{-1}$  and C–Cl at  $626\text{ cm}^{-1}$  [23]. The appearance of the C=N bond strongly confirms that the formation of the CNCs is attributed to the crosslinking polymerization of precursors driven by the Schiff base reaction. The XPS spectrum (Figure 1d) clearly reveals that the prepared CNCs are composed of carbon (C1s, 284.8 eV), nitrogen (N1s, 399.3 eV), oxygen (O1s, 531.2 eV), and chlorine (Cl2p, 200.5 eV) elements. The high-resolution C1s spectrum (Figure 1e) exhibits three peaks at 287.7, 285.7, and 284.5 eV, which are ascribed to C=O/C=N, C–N, and C–C bonds, respectively [24]. In addition, the high-resolution N1s spectrum (Figure 1f) presents two peaks at 398.7 and 400.9 eV, which are attributed to C=N and N–H bonds, respectively [25]. Moreover, three peaks at 532.7, 531.6, and 530.3 eV in the O1s spectrum (Figure 1g) can be attributed to the adsorbed  $\text{H}_2\text{O}$ , O–H, and C=O bonds, respectively [26,27]. Due to the spin-orbit splitting of the Cl2p core level, the Cl2p spectrum (Figure 1h) shows two peaks centered at 201.5 and 199.9 eV, which can be attributed to  $\text{Cl}2p_{1/2}$  and  $\text{Cl}2p_{3/2}$ , respectively [28]. These results demonstrate that the prepared CNCs are a kind of ultra-small amorphous carbon nanoparticles containing rich C=N and C≡N groups.

## 2.2. Optical Properties of CNCs

The optical properties of CNCs are investigated in detail by absorption and FL spectra. As shown in Figure 2a, the absorption spectrum of CNCs exhibits two strong absorption bands at 257 and 407 nm, which are due to the  $\pi-\pi^*$  transition of the conjugated  $\text{sp}^2$  structure and  $n-\pi^*$  transition of aggregated fluorescent groups [29]. Correspondingly, two excitation peaks have been found at 257 and 417 nm in the excitation spectrum of the CNCs. No matter if excited at 260 (channel 1) or 410 nm (channel 2), only one green emission peak of about 518 nm can be obtained, and there is only a diversity in intensity between the two. This unique dual-exciting central emission phenomenon is clearly displayed on a three-dimensional (3D) FL spectrum. The result (Figure 2b) shows that the CNCs show an excitation-independent green FL emission that can be excited at two excitation centers.

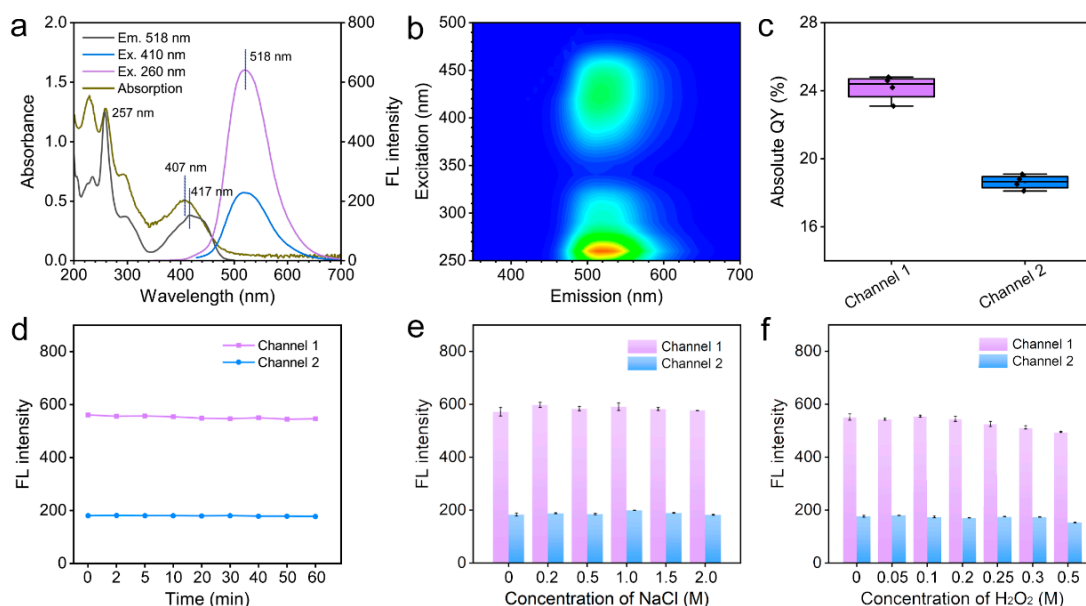


**Figure 2.** Optical properties and stability of dual-exciting central CNCs. (a) Absorption, excitation, and emission spectra, and (b) 3D FL spectrum of the CNCs. (c) Absolute QYs of the CNCs at different channels. (d) Photostability. (e) The stability in a salty medium, and (f) the antioxidant capacity of the CNCs.

Because of the lack of crystal structure, the strong green FL of the CNCs should be attributed to their surface state, rather than the quantum confinement effect [30]. The excitation peak of 257 nm may be ascribed to the  $\pi-\pi^*$  transition of the conjugated  $sp^2$  structure, while the excitation peak of 417 nm may be devoted to the  $n-\pi^*$  transition of N-related groups such as the C = N bond. The dual-exciting central emission feature may be due to the hyperconjugation of their two FL centers [31]. Meanwhile, the luminescent efficiency of the CNCs is excitation-dependent, and the absolute quantum yields (QYs) of the CNCs are about 24.2% for channel 1 and 18.6% for channel 2 (Figure 2c).

Stability is an important parameter of nanoprobe, which determines the accuracy of the sensing system [32]. The traditional dye molecules are usually photosensitive and can easily cause FL quenching under strong light irradiation. On the contrary, the proposed CNCs exhibit good photostability, and their FL intensities at two excitations remain unchanged under 60 min of UV irradiation (Figure 2d), suggesting that they can be used for long-term imaging and sensing. Meanwhile, the FL intensities of the CNCs are also almost constant in a high ionic strength medium of up to 2 M (Figure 2e). Additionally, the proposed CNCs possess good antioxidant ability, and their FL emissions are not affected by the high concentration of  $H_2O_2$  solution (Figure 2f). The solution pH has an important effect on the luminescence intensity of the CNCs. The result (Figure S1) shows that the FL intensities of CNCs at two excitations increase gradually with the increase in pH value from 1 to 11, which is usually due to the protonation and deprotonation of surface groups of CNCs controlled by the solution pH [21]. This result also indirectly indicates that the FL emission of the CNCs comes from the surface state.

### 2.3. Dual-Channel Fluorescent Detection of Hemin

Hemin can effectively quench the FL of the CNCs, which shows a channel-dependent quenching effect. The quenching process levels off after 1 min with the extension of the incubation time (Figure S2), suggesting that the sensing process is rapid. By using channel 1 (260 nm excitation), the ratio of the FL intensity of the CNCs is linearly correlated with the concentration of hemin in the range of 0.075–10  $\mu$ M, with a low limit of detection of about 30 nM (Figure 3a,b). Common interferents, such as  $Na^+$ ,  $Co^{2+}$ , L-glutathione (GSH), and cysteine (Cys) have little effect on the FL emission of CNCs in the absence and presence of hemin (Figure 3c), indicating that these interferents do not affect the detection of hemin by channel 1. By using channel 2 (410 nm excitation), the FL intensity ratio of the CNCs is proportional to the hemin concentration in the range of 0.25–10  $\mu$ M with a limit of detection of about 90 nM (Figure 3d,e). Likewise, these interferents also do not affect the detection of hemin by channel 2 (Figure 3f). In view of this, the proposed CNCs can serve as dual-channel sensing nanoprobe for the detection of hemin with good selectivity. Other methods for detecting hemin usually rely on a single signal (Table S1). Although the limit of detection of the proposed probes is not the lowest, the high selectivity and accurate detection results with self-supervision make them powerful sensing probes for the detection of hemin.

Subsequently, the quenching effect of dual-exciting central CNCs by hemin is explored. The inner filter effect is regarded as a non-radiative energy conversion process, which can be well used for the detection of analytes by competitive light absorption. A highly efficient inner filter effect usually requires a great spectral overlap between the absorption band of analytes and the excitation/emission band of nanoprobe [33]. The high selectivity of hemin detection is attributed to the fact that the absorption band of common interfering substances, such as GSH and Cys, is usually located in the deep ultraviolet region, which has no effect on the excitation and emission light of the CNCs and, therefore, does not interfere with the detection of hemin. As shown in Figure 4a, the absorption band of hemin has a greater overlap with the excitation band of channel 1 of CNCs in comparison to the excitation band of channel 2 of CNCs. This result shows that hemin can more effectively absorb the excitation light of channel 1 and achieve a more sensitive response. Moreover, no new absorption bands occur for the mixtures of CNCs and hemin, indicating that there

is no formation of new complexes between the CNCs and hemin (Figure 4b). Meanwhile, the FL decay curves (Figure 4c,d) of CNCs exhibit that there are almost no variations in a lifetime for CNCs in the absence and presence of hemin. These results strongly confirm that the FL quenching of the CNCs induced by hemin is due to the inner filter effect.

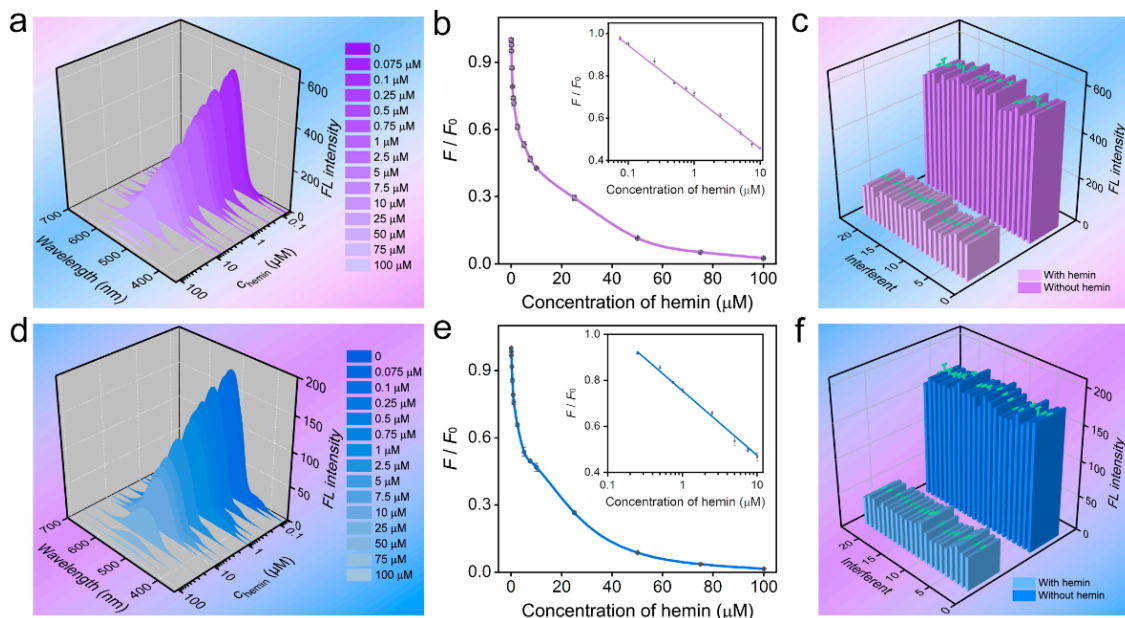


**Figure 3.** Sensitivity and selectivity of hemin detection. The FL spectra of CNCs in the presence of hemin excited at (a) 260 nm (channel 1) and (d) 410 nm (channel 2). Sensitivity of hemin detection by (b) channel 1 and (e) channel 2. FL responses of CNCs in the presence of 50  $\mu\text{M}$  interferents by (c) channel 1 and (f) channel 2. The columns represent the following: 1, control; 2,  $\text{Na}^+$ ; 3,  $\text{Mg}^{2+}$ ; 4,  $\text{K}^+$ ; 5,  $\text{Co}^{2+}$ ; 6,  $\text{Ni}^{2+}$ ; 7,  $\text{Cu}^{2+}$ ; 8,  $\text{Ag}^+$ ; 9,  $\text{Cd}^{2+}$ ; 10,  $\text{Ba}^{2+}$ ; 11,  $\text{Pb}^{2+}$ ; 12,  $\text{Cl}^-$ ; 13,  $\text{Pb}^{2+}$ ; 14,  $\text{HCO}_3^-$ ; 15,  $\text{H}_2\text{PO}_4^-$ ; 16, Lys; 17, Thr; 18, Val; 19, glucose; 20, dopamine; 21, Cys; 22, Hcy; 23, GSH. Concentration of hemin: 25  $\mu\text{M}$ . Error bars represent  $\pm$  S.D ( $n = 3$ ).

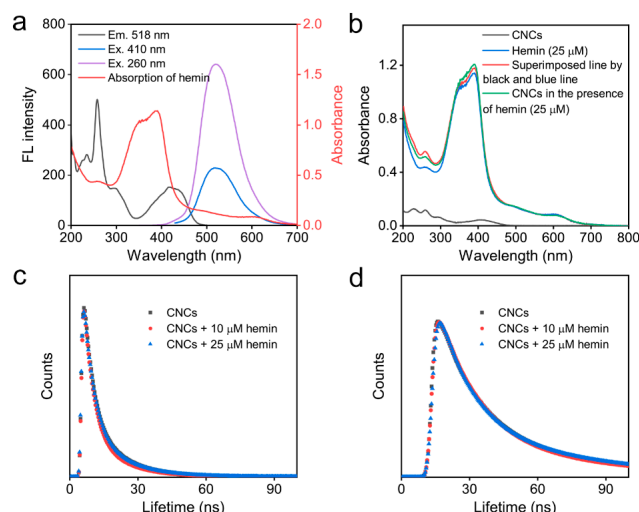


**Figure 4.** The sensing mechanism of hemin using CNCs. (a) Overlap degree of the absorption band of hemin and excitation and emission bands of CNCs at two channels. (b) The absorption spectra of CNCs in the absence and presence of hemin. (c) Time-resolved decay of CNCs before and after adding hemin (10 mM or 25 mM). Excitation: 260 nm. (d) Time-resolved decay of CNCs before and after adding hemin (10 mM or 25 mM). Excitation: 410 nm.

#### 2.4. Determination of Hemin in Cells

Before cell imaging, the cytotoxicity of CNCs is tested. The cytotoxicity of CNCs is relatively low based on the result of the CCK-8 assay assessment (Figure S3), and over 90% HeLa cell viability is observed after 24 h incubation with the CNCs (0.05–5 mg/mL). The real-time monitoring of the dynamic invasion process of hemin into HeLa cells is further investigated. As shown in Figure 5, HeLa cells display bright green FL after incubation with CNCs for 2 h, indicating that CNCs efficiently enter into the cells by endocytosis. Some reports reveal that both caveolae- and clathrin-mediated endocytosis is the main cellular uptake mechanism of nanocarbon [34], indicating that multiple endocytosis pathways may cause the high transfection efficiency of CNCs. After the addition of hemin for 30 min, the green FL of CNCs is effectively quenched, and the degree of quenching is closely related to the concentration of hemin. Therefore, the proposed CNCs can be used as fluorescent nanoprobes to monitor the dynamic intrusion process of hemin into cells.

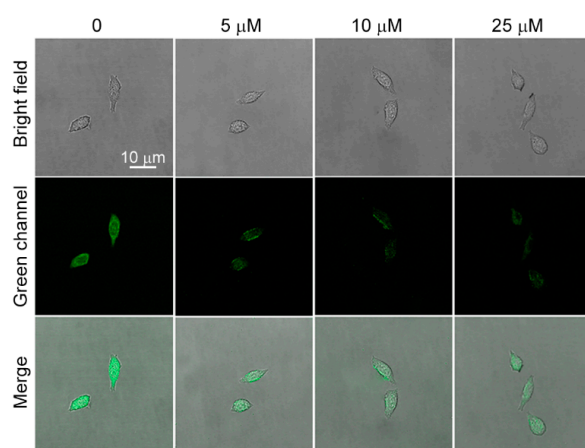


**Figure 5.** Laser confocal microscopic images of HeLa cells incubated with different concentrations of hemin. Excitation: 405 nm. Incubation time: 30 min. Concentration of CNCs: 1 mg/mL.

### 3. Materials and Methods

#### 3.1. Materials and Reagents

Dopamine, GSH, Cys, homocysteine (Hcy), DDQ, and EDA are obtained from Aladdin Reagent Co., Ltd. (Shanghai, China). Glucose, threonine (Thr), lysine (Lys), and valine (Val) are from Macklin Biochemical Co., Ltd. (Shanghai, China). All reagents are used without any further purification, which are dissolved in 18.2 MΩ.cm ultrapure water.

#### 3.2. Apparatus and Characterization

The morphology of CNCs is obtained by a Talos F200XTEM. The FL spectra of CNCs are measured by an F97Pro FL spectrophotometer. The absorption spectra of CNCs are measured by a 759S UV-Vis spectrophotometer. The FL lifetimes of CNCs are obtained by an FLS1000 FL spectrometer. The surface element composition of CNCs is determined using an XPS.

#### 3.3. Preparation and Purification of CNCs

The synthesis of CNCs is achieved by the Schiff base reaction between DDQ and EDA. Briefly, 10 mg DDQ and 0.3 mL EDA are added to 4.7 mL ultrapure water in turn. The CNCs can be formed after 5 days of room-temperature reaction. The proposed CNCs are dialyzed using a 100–500 MWCO dialysis membrane for 2 days.

#### 3.4. Sensing Procedure of Hemin Using CNCs

CNCs solution (20 μL) is firstly added to 1.78 mL water, and then different concentrations of hemin (0.2 mL) are further added. The above solution is incubated for 2 min and

then transferred to a quartz cell for FL measurement. The selectivity of CNCs nanoprobe is studied by adding various interferents such as ions ( $\text{Na}^+$ ,  $\text{Mg}^{2+}$ ,  $\text{K}^+$ ,  $\text{Co}^{2+}$ ,  $\text{Ni}^{2+}$ ,  $\text{Cu}^{2+}$ ,  $\text{Ag}^+$ ,  $\text{Cd}^{2+}$ ,  $\text{Ba}^{2+}$ ,  $\text{Pb}^{2+}$ ,  $\text{Cl}^-$ ,  $\text{HCO}_3^-$ , and  $\text{H}_2\text{PO}_4^-$ ), amino acids (Lys, Thr, and Val), and other substances (GSH, Cys, Hcy, dopamine, and glucose) that are used to replace hemin at a high concentration of 50  $\mu\text{M}$ . The excitation light is selected at 260 and 410 nm as the dual-channel signals for detection.

#### 4. Conclusions

In conclusion, a facile and one-pot Schiff base reaction is developed for the fabrication of dual-exciting central CNCs at room temperature. The excitation-independent green emission of CNCs can be excited at two different excitation regions (260 nm and 410 nm), showing the unique optical phenomenon of dual-excitation and single-emission. Additionally, the proposed CNCs with low toxicity exhibit good oxidation and photobleaching resistance. Based on the dual-exciting emission properties, CNCs can serve as dual-channel FL nanoprobe for the highly sensitive detection of hemin based on the inner filter effect. Meanwhile, CNCs display high reproducibility for sensing hemin in living cells, providing new insights to design a reliable dual-channel sensing nanoprobe for analytical and biomedical applications.

**Supplementary Materials:** The following supporting information can be downloaded at: <https://www.mdpi.com/article/10.3390/inorganics11060226/s1>, Figure S1: effect of solution pH on FL emissions of CNCs at two channels; Figure S2: relationship between FL intensity and incubation time; Table S1: the comparison of the determination of hemin [35,36]; Figure S3: the biocompatibility of the CNCs.

**Author Contributions:** Data curation, B.-B.C.; formal analysis, Y.-T.G. and S.C.; funding acquisition, D.-W.L.; methodology, Y.-T.G.; project administration, D.-W.L.; software, Y.-T.G.; supervision, B.-B.C. and D.-W.L.; validation, Y.-T.G.; visualization, B.-B.C.; writing—original draft, B.-B.C.; writing—review and editing, B.-B.C. and D.-W.L. All authors have read and agreed to the published version of the manuscript.

**Funding:** The authors appreciate the financial support from the National Natural Science Foundation of China (21974046, 22176058, and 21977031), the Science and Technology Commission of Shanghai Municipality (19520744000 and 19ZR1472300), and the Fundamental Research Funds for the Central Universities (222201717003).

**Data Availability Statement:** Not applicable.

**Acknowledgments:** The authors thank the Research Center of Analysis and Test of East China University of Science and Technology for the help with the characterization.

**Conflicts of Interest:** The authors declare no conflict of interest.

#### References

1. Liu, M.L.; Chen, B.B.; Li, C.M.; Huang, C.Z. Carbon dots prepared for fluorescence and chemiluminescence sensing. *Sci. China Chem.* **2019**, *62*, 968–981. [CrossRef]
2. Chen, B.B.; Liu, M.L.; Huang, C.Z. Recent advances of carbon dots in imaging-guided theranostics. *TrAC Trends Anal. Chem.* **2021**, *134*, 116116. [CrossRef]
3. Park, S.-H.; Kwon, N.; Lee, J.-H.; Yoon, J.; Shin, I. Synthetic ratiometric fluorescent probes for detection of ions. *Chem. Soc. Rev.* **2020**, *49*, 143–179. [CrossRef]
4. Gui, R.; Jin, H.; Bu, X.; Fu, Y.; Wang, Z.; Liu, Q. Recent advances in dual-emission ratiometric fluorescence probes for chemo/biosensing and bioimaging of biomarkers. *Coordin. Chem. Rev.* **2019**, *383*, 82–103. [CrossRef]
5. Chen, B.-B.; Liu, M.-L.; Gao, Y.-T.; Chang, S.; Qian, R.-C.; Li, D.-W. Design and applications of carbon dots-based ratiometric fluorescent probes: A review. *Nano Res.* **2023**, *16*, 1064–1083. [CrossRef]
6. Qian, J.; Ren, C.; Wang, C.; An, K.; Cui, H.; Hao, N.; Wang, K. Gold nanoparticles mediated designing of versatile aptasensor for colorimetric/electrochemical dual-channel detection of aflatoxin B1. *Biosens. Bioelectron.* **2020**, *166*, 112443. [CrossRef] [PubMed]
7. Li, W.; Zhang, X.; Hu, X.; Shi, Y.; Liang, N.; Huang, X.; Wang, X.; Shen, T.; Zou, X.; Shi, J. Simple design concept for dual-channel detection of Ochratoxin A based on bifunctional metal-organic framework. *ACS Appl. Mater. Interfaces* **2022**, *14*, 5615–5623. [CrossRef]

8. Wang, C.; Gao, X.; Wang, S.; Liu, Y. A smartphone-integrated paper sensing system for fluorescent and colorimetric dual-channel detection of foodborne pathogenic bacteria. *Anal. Bioanal. Chem.* **2020**, *412*, 611–620. [[CrossRef](#)]
9. Hang, L.; Zhou, F.; Men, D.; Li, H.; Li, X.; Zhang, H.; Liu, G.; Cai, W.; Li, C.; Li, Y. Functionalized periodic Au@MOFs nanoparticle arrays as biosensors for dual-channel detection through the complementary effect of SPR and diffraction peaks. *Nano Res.* **2017**, *10*, 2257–2270. [[CrossRef](#)]
10. Fereja, S.L.; Fang, Z.; Li, P.; Guo, J.; Fereja, T.H.; Chen, W. “Turn-off” sensing probe based on fluorescent gold nanoclusters for the sensitive detection of hemin. *Anal. Bioanal. Chem.* **2021**, *413*, 1639–1649. [[CrossRef](#)]
11. Gao, L.; Xiao, Y.; Wang, Y.; Chen, X.; Zhou, B.; Yang, X. A carboxylated graphene and aptamer nanocomposite-based aptasensor for sensitive and specific detection of hemin. *Talanta* **2015**, *132*, 215–221. [[CrossRef](#)] [[PubMed](#)]
12. Gao, S.; Wang, R.; Bi, Y.; Qu, H.; Chen, Y.; Zheng, L. Identification of frozen/thawed beef based on label-free detection of hemin (Iron Porphyrin) with solution-gated graphene transistor sensors. *Sens. Actuators B Chem.* **2020**, *305*, 127167. [[CrossRef](#)]
13. Du, N.; Zhang, H.; Wang, J.; Dong, X.; Li, J.; Wang, K.; Guan, R. Fluorescent silicon nanoparticle-based quantitative hemin assay. *Anal. Bioanal. Chem.* **2022**, *414*, 8223–8232. [[CrossRef](#)] [[PubMed](#)]
14. Zhao, L.; Chen, F.; Huang, W.; Bao, H.; Hu, Y.; Huang, X.-a.; Deng, T.; Liu, F. A fluorescence turn-on assay for simple and sensitive determination of hemin and blood stains. *Sens. Actuators B Chem.* **2020**, *304*, 127392. [[CrossRef](#)]
15. Ni, P.; Chen, C.; Jiang, Y.; Lu, Y.; Chen, W. A simple and sensitive fluorescent assay for hemin detection based on artemisinin-thiamine. *Sens. Actuators B Chem.* **2018**, *273*, 198–203. [[CrossRef](#)]
16. Fereja, T.H.; Kitte, S.A.; Gao, W.; Yuan, F.; Snizhko, D.; Qi, L.; Nsabimana, A.; Liu, Z.; Xu, G. Artesunate-luminol chemiluminescence system for the detection of hemin. *Talanta* **2019**, *204*, 379–385. [[CrossRef](#)]
17. Bushira, F.A.; Kitte, S.A.; Xu, C.; Li, H.; Zheng, L.; Wang, P.; Jin, Y. Two-dimensional-plasmon-boostered iron single-atom electrochemiluminescence for the ultrasensitive detection of dopamine, hemin, and mercury. *Anal. Chem.* **2021**, *93*, 9949–9957. [[CrossRef](#)]
18. Li, D.; Li, C.; Liang, A.; Jiang, Z. SERS and fluorescence dual-mode sensing trace hemin and K<sup>+</sup> based on G-quarplex/hemin DNAzyme catalytic amplification. *Sens. Actuators B Chem.* **2019**, *297*, 126799. [[CrossRef](#)]
19. Liu, M.L.; Yang, L.; Li, R.S.; Chen, B.B.; Liu, H.; Huang, C.Z. Large-scale simultaneous synthesis of highly photoluminescent green amorphous carbon nanodots and yellow crystalline graphene quantum dots at room temperature. *Green Chem.* **2017**, *19*, 3611–3617. [[CrossRef](#)]
20. Chang, S.; Chen, B.B.; Lv, J.; Fodjo, E.K.; Qian, R.C.; Li, D.W. Label-free chlorine and nitrogen-doped fluorescent carbon dots for target imaging of lysosomes in living cells. *Microchim. Acta* **2020**, *187*, 435–442. [[CrossRef](#)]
21. Chen, B.B.; Liu, Z.X.; Deng, W.C.; Zhan, L.; Liu, M.L.; Huang, C.Z. A large-scale synthesis of photoluminescent carbon quantum dots: A self-exothermic reaction driving the formation of the nanocrystalline core at room temperature. *Green Chem.* **2016**, *18*, 5127–5132. [[CrossRef](#)]
22. Gao, Y.-T.; Chen, B.-B.; Jiang, L.; Lv, J.; Chang, S.; Wang, Y.; Qian, R.-C.; Li, D.-W.; Hafez, M.E. Dual-emitting carbonized polymer dots synthesized at room temperature for ratiometric fluorescence sensing of vitamin B12. *ACS Appl. Mater. Interfaces* **2021**, *13*, 50228–50235. [[CrossRef](#)]
23. Marković, Z.M.; Labudová, M.; Danko, M.; Matijašević, D.; Mičušík, M.; Nádaždy, V.; Kováčová, M.; Kleinová, A.; Špitalský, Z.; Pavlović, V.; et al. Highly efficient antioxidant F<sup>-</sup> and Cl<sup>-</sup>-doped carbon quantum dots for bioimaging. *ACS Sustain. Chem. Eng.* **2020**, *8*, 16327–16338. [[CrossRef](#)]
24. Liu, M.L.; Chen, B.B.; He, J.H.; Li, C.M.; Li, Y.F.; Huang, C.Z. Anthrax biomarker: An ultrasensitive fluorescent ratiometry of dipicolinic acid by using terbium(III)-modified carbon dots. *Talanta* **2019**, *191*, 443–448. [[CrossRef](#)]
25. Stevens, J.S.; de Luca, A.C.; Pelendritis, M.; Terenghi, G.; Downes, S.; Schroeder, S.L.M. Quantitative analysis of complex amino acids and RGD peptides by X-ray photoelectron spectroscopy (XPS). *Surf. Interface Anal.* **2013**, *45*, 1238–1246. [[CrossRef](#)]
26. Klopogge, J.T.; Duong, L.V.; Wood, B.J.; Frost, R.L. XPS study of the major minerals in bauxite: Gibbsite, bayerite and (pseudo-) boehmite. *J. Colloid Interface Sci.* **2006**, *296*, 572–576. [[CrossRef](#)]
27. Yang, D.; Velamakanni, A.; Bozoklu, G.; Park, S.; Stoller, M.; Piner, R.D.; Stankovich, S.; Jung, I.; Field, D.A.; Ventrice, C.A., Jr. Chemical analysis of graphene oxide films after heat and chemical treatments by X-ray photoelectron and Micro-Raman spectroscopy. *Carbon* **2009**, *47*, 145–152. [[CrossRef](#)]
28. Gu, J.; Hu, M.J.; Guo, Q.Q.; Ding, Z.F.; Sun, X.L.; Yang, J. High-yield synthesis of graphene quantum dots with strong green photoluminescence. *RSC Adv.* **2014**, *4*, 50141–50144. [[CrossRef](#)]
29. Bai, L.; Yan, H.; Feng, Y.; Feng, W.; Yuan, L. Multi-excitation and single color emission carbon dots doped with silicon and nitrogen: Synthesis, emission mechanism, Fe<sup>3+</sup> probe and cell imaging. *Chem. Eng. J.* **2019**, *373*, 963–972. [[CrossRef](#)]
30. Liu, M.L.; Chen, B.B.; Li, C.M.; Huang, C.Z. Carbon dots: Synthesis, formation mechanism, fluorescence origin and sensing applications. *Green Chem.* **2019**, *21*, 449–471. [[CrossRef](#)]
31. Liao, X.; Chen, C.; Yang, J.; Zhou, R.; Si, L.; Huang, Q.; Huang, Z.; Lv, C. Nitrogen-doped carbon dots for dual-wavelength excitation fluorimetric assay for ratiometric determination of phosalone. *Microchim. Acta* **2021**, *188*, 247. [[CrossRef](#)] [[PubMed](#)]
32. Chen, B.B.; Liu, H.; Huang, C.Z.; Ling, J.; Wang, J. Rapid and convenient synthesis of stable silver nanoparticles with kiwi juice and its novel application for detecting protease K. *New J. Chem.* **2015**, *39*, 1295–1300. [[CrossRef](#)]
33. Chen, S.; Yu, Y.L.; Wang, J.H. Inner filter effect-based fluorescent sensing systems: A review. *Anal. Chim. Acta* **2018**, *999*, 13–26. [[CrossRef](#)]

34. Cao, X.; Wang, J.P.; Deng, W.W.; Chen, J.J.; Wang, Y.; Zhou, J.; Du, P.; Xu, W.Q.; Wang, Q.; Wang, Q.L.; et al. Photoluminescent cationic carbon dots as efficient non-viral delivery of plasmid SOX9 and chondrogenesis of fibroblasts. *Sci. Rep.* **2018**, *8*, 7057. [[CrossRef](#)] [[PubMed](#)]
35. Kang, B.H.; Li, N.; Liu, S.G.; Li, N.B.; Luo, H.Q. A label-free, highly sensitive and selective detection of hemin based on the competition between hemin and protoporphyrin IX binding to G-quadruplexes. *Anal. Sci.* **2016**, *32*, 887–892. [[CrossRef](#)] [[PubMed](#)]
36. Guo, Z.; Li, B.; Zhang, Y.; Zhao, Q.; Zhao, J.; Li, L.; Zuo, G. Acid-treated Graphitic Carbon Nitride Nanosheets as Fluorescence Probe for Detection of Hemin. *ChemistrySelect* **2019**, *4*, 8178–8182. [[CrossRef](#)]

**Disclaimer/Publisher's Note:** The statements, opinions and data contained in all publications are solely those of the individual author(s) and contributor(s) and not of MDPI and/or the editor(s). MDPI and/or the editor(s) disclaim responsibility for any injury to people or property resulting from any ideas, methods, instructions or products referred to in the content.